HHS Public Access

Author manuscript

Sci Transl Med. Author manuscript; available in PMC 2023 November 26.

Published in final edited form as:

Sci Transl Med. 2023 April 19; 15(692): eadf4086. doi:10.1126/scitranslmed.adf4086.

Rescue of glutaric aciduria type I in mice by liver-directed therapies

Mercedes Barzi[1], **Collin G. Johnson**[2], **Tong Chen**[1], **Ramona M. Rodriguiz**[3], **Madeline Hemmingsen**[1], **Trevor J Gonzalez**[4], **Alan Rosales**[4], **James Beasley**[1], **Cheryl K. Peck**[5], **Yunhan Ma**[1], **Ashlee R. Stiles**[1], **Timothy C. Wood**[5], **Raquel Maeso-Diaz**[6], **Anna Mae Diehl**[6], **Sarah P. Young**[1], **Jeffrey I. Everitt**[7], **William C. Wetsel**[3], **William R. Lagor**[8], **Beatrice Bissig-Choisat**[1], **Aravind Asokan**[4,9,10,11], **Areeg El-Gharbawy**[1], **Karl-Dimiter Bissig**[1,6,10,11,12,§]

[1]Alice and Y. T. Chen Center for Genetics and Genomics, Division of Medical Genetics, Department of Pediatrics, Duke University Medical Center, Durham, NC 27710, USA

[2]Center for Cell and Gene Therapy, Stem Cells and Regenerative Medicine Center, Baylor College of Medicine, Houston, TX 77030, USA

[3]Department of Psychiatry and Behavioral Sciences, Cell Biology and Neurobiology, Mouse behavioral and Neuroendocrine Analysis Core Facility Duke University Medical Center, Durham, NC 27710, USA

[4]Department of Molecular Genetics and Microbiology, Duke University Medical Center, Durham, NC 27710, USA

[5]Biochemical Genetics Laboratory, Children's Hospital Colorado Anschutz Medical Campus, Co 80045, USA

[6]Division of Gastroenterology, Department of Medicine, Duke University Medical Center, Durham, NC 27710, USA

[7]Department of Pathology, Duke University Medical Center, Durham, NC 27710, USA

[8]Department of Integrative Physiology, Baylor College of Medicine, Houston, TX 77030, USA

[9]Department of Surgery, Duke University Medical Center, Durham, NC 27710, USA

[10]Department of Biomedical Engineering (BME) at the Duke University Pratt School of Engineering, Durham, NC 27710, USA

[11]Duke Cancer Center, Duke University Medical Center, Durham, NC 27710, USA

[§]Corresponding author.

Author contributions: K.D.B., M.B. and C.G.J. designed the experiments. A.E.G., A.A., S.Y., and W.R.L., gave conceptual input. M.B and C.G.J. did primary data analysis, M.B., C.J. and B.B.C. performed *in vivo* experiments. C.G.J. designed and crossed the knockout models. R.M and A.M.D. helped with isolation of mouse hepatocytes. T.J.G and A.R produced the AAV viruses. T.C., M.H. and A.M. helped with monitoring and harvesting of mice. T.C. did the Western blots. S.Y, J.B and A.R.S did C5-DC analysis. T.W did GA and 3-OH-GA analysis. W.C.W and R.M.R. designed and performed the neurobehavioral assays. J.I.E did the histopathological analysis. All authors read and approved the final manuscript.

Competing interests: M.B., C.G.J. and K.D.B. are inventors on patent application PCTUS2276982, "Compositions For And Methods Of Treating And/Or Preventing Glutaric Aciduria Type-I". The other authors have no competing interests to declare.

Overline: INBORN ERRORS OF METABOLISM

[12]Department of Pharmacology and Cancer Biology, Duke University Medical Center, Durham, NC 27710, USA

Abstract

Glutaric Aciduria Type I (GA-1) is an inborn error of metabolism with a severe neurological phenotype caused by the deficiency of glutaryl-CoA dehydrogenase (*GCDH*), the last enzyme of lysine catabolism. Current literature suggests that toxic catabolites in the brain are produced locally and do not cross the blood brain barrier. In a series of experiments using knockout mice of the lysine catabolic pathway and liver cell transplantation, we uncovered that toxic GA-1 catabolites in the brain originated from the liver. Moreover, the characteristic brain and lethal phenotype of the GA-1 mouse model was rescued by two different liver-directed gene therapy approaches: using an Adeno-Associated Virus (AAV) we replaced the defective *Gcdh* gene, or we prevented flux through the lysine degradation pathway by CRISPR deletion of the aminoadipate-semialdehyde synthase (*Aass)* gene. Our findings question the current pathophysiological understanding of GA-1 and reveal a targeted therapy for this devastating disorder.

One sentence summary:

Manipulation of lysine catabolism in the liver rescues glutaric aciduria and prevents metabolic and neuro-pathological phenotypes.

Introduction

The essential amino acid lysine is a building block of proteins but is also catabolized to glutaryl-CoA, which eventually enters the tricarboxylic acid cycle and generates energy. If the conversion of lysine to glutaryl-CoA is inhibited by a deficiency of the glutaryl-CoA dehydrogenase (GCDH) enzyme, disease-specific catabolites such as glutaric acid (GA) and 3-hydroxy-glutaric acid (3-OH-GA) accumulate (Fig. 1A). These intermediates accumulate in the brain where clinical symptoms develop that comprise a disorder known as glutaric aciduria type I (GA-1) (1). Striatal injury leads to complex movement disorders and subdural or other hemorrhages. Infection, fasting, or other physiological stress can trigger an encephalopathic crisis with poor prognosis. Extracerebral symptoms are rare, but occasionally chronic renal failure is observed, typically in older patients (2). The most critical phase of this disorder is the first six years of life, and because early treatment can effectively reduce the associated high mortality and morbidity, GA-1 is included in many countries' newborn screens. The standard of care for patients with GA-1 is strict dietary restriction of lysine, carnitine supplementation, and emergency support during decompensation. Despite early diagnosis and prospective care, 25–33% of all patients still suffer-long term neurological disabilities (3, 4). Currently there is no specific therapy available for GA-1, which might be a result of our incomplete understanding of its pathogenesis.

Among the scientific community, it is widely accepted that toxic catabolites accumulate locally and do not cross the blood-brain barrier (2, 5–7). GA and 3-OH-GA are believed to

be retained in the brain with limited efflux as reactive acyl-CoA species (Fig. 1A), leading to toxicity in neurons. Hence, the cornerstone of current therapy is substrate reduction, for example dietary restriction of lysine, which normally enters the brain via the solute carrier family 7 member 1 transporter (SLC7A1).

With the knowledge that toxic catabolites originating from the liver can accumulate in the brain in other amino acid disorders (8, 9), we conducted a series of transplantation experiments to investigate the orgin of toxic metabolites in GA-1. We demonstrate that GA and OH-GA can cross the blood-brain barrier and accumulate in the brain of Gcdh$^{-/-}$ mice, a mouse model of GA-1, thereby challenging the current dogma that toxic metabolites in this disease originate in the brain. Typical neuropathological alterations were observed even in the absence of lysine catabolism in the murine brain. This mechanistic insight allowed us to develop liver-directed therapeutic approaches for GA-1.

Results

Generation of *Gcdh*$^{-/-}$ mice and hepatocyte transplantation.

The *Gcdh*$^{-/-}$ mouse is a well-characterized animal model for GA-1 (10)(11). These mice die after only a few days on high-protein (casein) diet, developing a neuronal phenotype with hippocampal vacuolation and meningeal hemorrhage (12, 13). However, because this diet-induced sensitivity is dependent on the mouse background strain (13) and we wanted to explore hepatocyte transplantation in *Gcdh*$^{-/-}$ mice, we generated two *Gcdh*$^{-/-}$ strains. We deleted the *Gcdh* gene in zygotes of C57BL/6 and TIRF (*transgene free Il2rg*$^{-/-}$/*Rag2*$^{-/-}$/*Fah*$^{-/-}$) mice using CRISPR (Fig. S1). We previously successfully used the latter strain for hepatocyte transplantation and replacement of the host liver (14, 15). Both strains displayed the typical symptoms associated with high protein-diet in the brain (Fig. 1B and 1C) without any obvious pathology in the liver and kidney (Fig. S2) as described previously (10, 11).

To elucidate the role of the liver in GA-1 pathogenesis, we first transplanted healthy hepatocytes (*Gcdh*$^{+/+}$) into *Gcdh*$^{-/-}$ mice and put them on high-protein diet after liver repopulation. As expected, the non-transplanted *Gcdh*$^{-/-}$ mice died after only a few days on high-protein diet. However, about half of the transplanted mice survived the dietary challenge (Fig. 1D). Surviving transplanted mice were euthanized after 170 days and analyzed for GA-1 catabolites in the liver and brain (Fig.1E and 1F). GA-1 catabolite concentrations were comparable to healthy mice not only in the liver but also in the brain, despite continued GCDH deficiency in the brain. Moreover, the neuronal vacuolation and meningeal hemorrhage characteristic of the *Gcdh*$^{-/-}$ mouse model was not observed in transplanted mice (Fig 1G, 1H and 1I) and motor performance was comparable to wild-type mice (Fig. S3). Liver immunostaining of transplanted mice that did not survive dietary challenge revealed unsuccessful transplantation (<5% repopulation) in all 6 mice, whereas all surviving transplanted mice (n=5) had an almost complete (>70%) repopulation with healthy hepatocytes (Fig. 1J and 1K). This experiment indicates that the biochemical and histological phenotype in the brain of *Gcdh*$^{-/-}$ mice can be reverted by restoration of normal lysine catabolism in the liver.

Generation of double knockout (*Gcdh*$^{-/-}$/*Aass*$^{-/-}$) mice and hepatocyte transplantation

To further investigate the disease mechanism, we asked whether GCDH deficiency in liver could lead to an accumulation of GA-1 catabolites in brains lacking lysine catabolism, hence in the absence of neuronal production of lysine catabolites. To answer this question, we first generated a double knockout mouse by deleting both *Gcdh* and the gene encoding the first enzyme in the lysine catabolic pathway, aminoadipic semialdehyde synthase (*Aass*) (Fig. S4). double knockout mice (*Gcdh*$^{-/-}$/*Aass*$^{-/-}$) exposed to a high-protein diet survived (Fig. 2A), with no obvious disease phenotype and only a small elevation of GA-1 catabolites (Fig. 2B and 2C). This is in agreement with a previous report showing that the pipecolate pathway generates minimal amounts of lysine catabolites (16). We next transplanted diseased GA-1 hepatocytes (*Gcdh*$^{-/-}$/*Aass*$^{+/+}$) into double knockout mice (*Gcdh*$^{-/-}$/*Aass*$^{-/-}$). The transplanted mice only survived a few days on the high-protein diet (Fig. 2D) and accumulated high amounts of catabolites in the liver and brain after only a few days (Fig. 2E and 2F). Only mice with high repopulation of diseased hepatocytes expired on a high protein diet (Fig. 2G and 2H). Similarly to non-transplanted *Gcdh*$^{-/-}$ mice, transplanted double knockout mice developed increased vacuolation in the brain (Fig. 2I, 2J and 2K.).

Transplantation of diseased *Gcdh*$^{-/-}$ hepatocytes to generate a liver-specific GA-1 mouse model

We next transplanted diseased *Gcdh*$^{-/-}$ hepatocytes (*Aass*$^{+/+}$ wild-type) into TIRF mice, which have normal lysine catabolism (*Gcdh*$^{+/+}$/*Aass*$^{+/+}$). In this liver-specific GA-1 model, mice did not succumb to a high protein diet (Fig. 3A) despite efficient liver repopulation with diseased hepatocytes (Fig. 3B). GA and OH-GA were elevated in the liver as expected, but not in the brain (Fig. 3C, D). In summary, these transplantation experiments demonstrate that in the absence of functional lysine catabolism in the brain, toxic catabolites from the liver accumulate in the brain and lead to the typical neurological symptoms of the GA-1 disease model.

Liver-directed gene replacement therapy for *Gcdh*$^{-/-}$ mice

The above mechanistic insights imply that liver directed therapies might be beneficial in *Gcdh*$^{-/-}$ mice. Therefore, we generated an Adeno-Associated Virus (AAV)-based gene therapy vector expressing under the control of a liver-specific promoter either wild-type *Gcdh* or green fluorescent protein (*GFP*) as a control (Fig. S5). We intravenously injected 3-week-old *Gcdh*$^{-/-}$ mice with the AAV vector at a dose of 1.5×10^{12} vg/mouse. Two weeks after injection mice were placed on a high-protein diet. Most mice were rescued from lethality and survived beyond at least four months (Fig. 4A) with expression of *Gcdh* in the liver but not in the brain (Fig. 4B). Immunostaining of rescued mice identified 70–95% hepatocytes as expressing GCDH (Fig. 4C). Glutarylcarnitine (C5-DC) concentrations in the blood (Fig. 4D), as well as GA (Fig. 4E) and 3-OH-GA (Fig. 4F) concentrations in brain and liver, indicated a biochemical reduction of lysine metabolites upon treatment with the liver-directed AAV-*Gcdh*.

In addition, neuronal vacuolation and meningeal hemorrhage were decreased in AAV-*Gcdh* treated compared to control *Gcdh*$^{-/-}$ mice (Fig. 4G, 4H, 4I). The motor performance of treated mice was comparable to C57BL/6 wild-type mice (Fig. S6). Because patients with

GA-1 ideally need to start treatment as neonates, we injected neonatal *Gcdh*$^{-/-}$ mice with a low (3×10^{11} vg/mouse), intermediate (7.5×10^{11} vg/mouse), or high (1.5×10^{12} vg/mouse) dose of AAV-*Gcdh*. After weaning, the treated mice were exposed to a high-protein diet. Although we observed a dose-dependent therapeutic effect, treatment of neonates was less durable than injecting *Gcdh*$^{-/-}$ mice at 3 weeks of age (Fig. 4J). This could be explained by a dose-dependent but overall lower expression of GCDH in the liver (Fig. 4K) of neonatally injected *Gcdh*$^{-/-}$ mice compared to those treated after weaning. The low proportion (2–10%) of GCDH-expressing hepatocytes (Fig. 4L) implies that after neonatal administration, the AAV vector may be diluted or silenced upon growth of the liver despite injection at a much higher dose per body weight. Hence, a more refined approach consisting of repeated treatment with AAV-*Gcdh* may further improve the therapeutic effect in neonatal *Gcdh*$^{-/-}$ mice.

Deletion of *Aass* in the liver by CRISPR gene therapy in *Gcdh*$^{-/-}$ mice

Last, to explore an alternative therapy for *Gcdh*$^{-/-}$ pups and to leverage our observation that transgenic deletion of *Aass* rescues the lethality of *Gcdh* deletion, we designed an AAV gene therapy vector expressing liver-directed CRISPR/Cas9 effector molecules targeting and thereby deleting Aass (Fig. S7). Again, we injected neonatal *Gcdh*$^{-/-}$ mice with a low (2.4×10^{11} vg/mouse), intermediate (6×10^{11} vg/mouse), or high (1×10^{12} vg/mouse) dose of the AAV vector. The high dose of AAV-*CRISPR* rescued all six injected pups from lethality induced by high protein diet after weaning (Fig. 5A). Biochemical analysis revealed a substantial reduction of lysine catabolites in both liver and brain (Fig. 5B and 5C) after 60 days on high-protein diet compared to AAV-*GFP* treated mice after only 4 days on high protein. AAV-CRISPR therapy resulted in a dose-dependent deletion of *Aass* in the liver (Fig. 5D). Hippocampal vacuolation and subdural hemorrhage were not observed in AAV-CRISPR-treated *Gcdh*$^{-/-}$ mice in contrast to clear pathological alterations in non-treated mice after only 4 days of high-protein diet exposure (Fig. 5E, 5F and 5G). Prior to euthanizing the AAV-CRISPR-treated *Gcdh*$^{-/-}$ mice, we conducted neurobehavioral testing and could only detect a mild reduction in the hind-paw grip strength compared to inbred C57BL/6 control mice (Fig. S8). Serum lysine concentrations were not significantly ($p>0.4$) increased (Fig. S9), despite the lack of hepatic lysine catabolism. As a proof-of-concept for knockdown instead of deletion, we targeted *Aass* by siRNA and observed a modest but significant ($p=0.02$) increase of survival of *Gcdh*$^{-/-}$mice with a one-time injection (Fig. S10). In summary, these results demonstrate that *Aass* deletion or reduction in the liver of neonates is therapeutic for *Gcdh*$^{-/-}$ mice, and a single injection of AAV-CRISPR protects mice from death or development of severe neurological symptoms.

Discussion

In a series of transplantation experiments we demonstrated that hepatic lysine catabolism directly impacts the accumulation of toxic catabolites in the brain in both directions (reduction or increase of catabolites) in the absence of functional lysine catabolism in the brain. These results are striking, given the previously described fruit bat (17) and liver-specific GA-1 mouse model (5), which both have a GCDH-deficiency in the liver but do not have any disease symptoms nor accumulation of catabolites in the brain. We reproduced

the same results when generating a liver-specific GA-1 mouse model with our TIRF strain. Moreover, isotope tracing experiments in C57BL/6 mice demonstrated an extremely limited accumulation in the brain after intraperitoneal injection of GA-1 catabolites (5). However, it is important to note that all these reports use animals with a functional lysine catabolism in the brain (for example *Gcdh*$^{+/+}$/*Aass*$^{+/+}$). In all these settings, the lack of neurotoxicity could be explained either by a reduced flux of GA-1 catabolites across the blood-brain barrier or by an efficient detoxification of GA-1 catabolites in the brain even when these catabolites originated from the liver. Our findings clearly support the latter interpretation and are compatible with all previous observations in bats or mice. Also, results from the earlier mouse studies (18) and human Genotype-Tissue Expression (GTEx) project show abundant expression of lysine catabolic genes in relevant brain areas (19) implying efficient cerebral lysine catabolism. In addition to revealing mechanistic insight into the obscure GA-1 pathology (20), our transplantation studies provide a scientific rationale for a liver-directed therapeutic approach.

We have recently developed a therapeutic concept called *metabolic pathway reprogramming* that couples CRISPR technology with a strategy from pharmacology, namely, to inhibit an enzymatic pathway rather than to edit a disease-causing gene directly (21). In our first proof of principle study, we rescued the lethality of hereditary tyrosinemia type I by liver-specific-deletion of the upstream enzyme hydroxyphenylpyruvate dioxygenase (22). However, in contrast to tyrosinemia, there is no small molecule inhibitor or other specific therapy for GA-1 and we believe that our AAV-CRISPR therapy could indeed be useful in the clinic. However, although gene editing is promising, there are some major clinical hurdles to overcome, such as off-target editing or expression of bacterial proteins in humans. It is conceivable that more readily translatable therapies such as siRNA or antisense oligonucleotide therapeutics could be developed in the current setting.

Nonetheless, we show that an AAV gene replacement therapy in the liver is a potential therapeutic option for GA-1. A few months ago, the first liver-directed AAV gene therapy was approved, with many other ongoing clinical trials targeting the liver using a gene replacement approach. Despite these encouraging advancements in AAV gene therapy, animal studies have identified an increased incidence of liver cancer after AAV-based treatment (23, 24) and at present it has not been determined if these observations also apply to humans. It is conceivable that mRNA therapies could circumvent this potential limitation, but come with limitations of their own. It is possible that both liver-directed therapies presented here could complement or substitute current dietary approaches, particularly for patients with compliance issues or for the prevention of long-term sequalae.

In summary, we have demonstrated in a series of transplantation experiments that the liver directly contributes to the toxic accumulation and therapeutic reduction of lysine catabolites in the brain. Further studies will be needed to identify the actual metabolites crossing the blood-brain barrier that are responsible for these observations and dissect the relative contributions of other pathomechanisms of GA-1 such as vascular dysfunction (25). Nevertheless, this mechanistic insight identifies an accessible organ to target for the development of therapeutics to eventually help patients suffering from GA-1.

Materials and Methods

Study design

This study aimed to elucidate the role of hepatic lysine catabolism with respect to the pathophysiology of GA-1 and develop a targeted therapy for this devastating disorder. Therefore, we designed a two-step procedure:

Hepatocyte transplantation experiments—Single and double knockout mice were transplanted and enriched with different knockout and wild-type hepatocytes as described under experiments and methods. After repopulation, animals were subjected to high-protein (casein) diet and used for all different experiments described in manuscript. Primary endpoints were survival, GA-1 catabolites, neuropathology, and motor performance.

Therapeutic approaches—Neonatal or adult single (Gcdh−/−) knockout mice were treated with two different gene therapy approaches (AAV-*Gcdh* or AAV-CRISPR). Doses and routes were as explained in the different experiments. After weaning of mice or two weeks after injection (adult), mice were put on a high-protein diet. Identical endpoints as described above were used. An additional siRNA treatment group was included with a one-time injection as described in methods. Primary endpoint of this group was survival and knockout efficiency by immunostaining for AASS.

Generation of single (*Gcdh*$^{-/-}$) and double (*Gcdh*$^{-/-}$ /*Aass*$^{-/-}$) knockout mouse models

Gcdh$^{-/-}$ single knockout and *Gcdh*$^{-/-}$ /*Aass*$^{-/-}$ double knockout mouse strains were generated by injecting either C57BL/6J or TIRF (transgene-free *Il2rg*$^{-/-}$, *Rag2*$^{-/-}$, *Fah*$^{-/-}$) zygotes (14, 15) with CRISPR/Cas9 gene editing mRNA as described previously (15). The following sgRNAs were designed using Benchling software and injected at the same time with the Cas9 mRNA: Gcdh (exon 3) – GCCGCTCCTGGCAGTAGTTA, Gcdh (exon 5) – GTGTGTCGTCGGTGGCCTAT, Aass (exon 6) – GTGCAGGCTGTCCGTGATGC, Aass (exon 7) – GAAACTTCTCTTAATTCGTG. F0 mice were analyzed by PCR followed by Sanger sequencing using the following PCR primers: *Gcdh* forward: TTATCCCCAGGGTCAGAAG, *Gcdh* reverse: CCAGACCGACATCTGAC, Aass forward: TAGAGAGAACGGGCAGGATGT, Aass reverse: TCTACGGGATCGTACACACCA. Further offspring genotyping was performed by Transnetyx.

Experiments with knockout mice

Control animals for experiments were C57BL/6J mice (#000664; Jackson Laboratories). Transplantation experiments were all conducted on the TIRF genetic background (14), whereas all other experiments were conducted on the C57BL/6J genetic background. Single (*Gcdh*$^{-/-}$) and double (*Gcdh*$^{-/-}$ /*Aass*$^{-/-}$) knockout mice were maintained under a standard 12-h dark/light cycle with water and regular chow provided *ad libitum*. Because our standard mouse chow is relatively poor in protein (21%) and mice have no protein-rich meals but constant access to food (no fasting), we used a high-protein diet (61% protein - 70% Casein diet; Envigo Teklad Custom diet) to trigger the disease phenotype. For AAV experiments, 3-week-old and 6-day-old *Gcdh*$^{-/-}$ pups were injected (i.p.) with a single concentration of AAV expressing either the murine *Gcdh* cDNA or with two CRISPR/Cas9 gene editing tools

targeting *Aass*, both regulated by a liver-specific promoter (*HLP*). Two weeks after injection or when pups reached the weaning age, mice were exposed to a high-protein diet.

For transplantation experiments (TIRF background) with ($Gcdh^{-/-}$) and double ($Gcdh^{-/-}$/$Aass^{-/-}$) knockout mice, 3-week-old mice were transplanted with $Gcdh^{-/-}$ or $Gcdh^{+/+}$ hepatocytes, respectively. Nitisinone was stepwise reduced over 8 days, and mice were kept for 5 months without drug treatment (during the expansion phase of hepatocytes) before being exposed to high-protein diet. Aged-matched controls were used for all transplant experiments. Urine, blood, liver, and brain (where described) were collected 4 or 5 days after challenging the mice with the high-protein diet. Mouse body weights were monitored throughout and all mouse tissues were collected for further analysis at the experimental endpoints. All animal experiment protocols were approved by the Duke University or Baylor College of Medicine Institutional Animal Care and Use Committee.

Hepatocyte isolation

To obtain primary hepatocytes for transplantation experiments, mouse livers were perfused using a modified two-step collagenase perfusion method as described previously (26). The quality of the isolated hepatocytes was assessed by trypan-blue staining of perfusate and used if viability was >90%. Freshly isolated hepatocytes were transplanted into mice the same day (<8 hours after isolation).

Hepatocyte transplantation

Hepatocyte transplantation was performed as previously described (27) in the TIRF genetic background host strain (*Transgene-free* $Il2^{-/-}/Rag2^{-/-}/Fah^{-/-}$). Healthy hepatocytes ($Gcdh^{+/+}$) expressing td-Tomato red fluorescent reporter (mT/mG mouse strain, B6.129(Cg)-Gt(ROSA)26Sor$^{tm4(ACTB-tdTomato,-EGFP)Luo/J}$, cat#007676; Jackson Laboratories) were used for the single knockout ($Gcdh^{-/-}$) mouse strain, and diseased ($Gcdh^{-/-}$) hepatocytes were transplanted into the double knockout ($Gcdh^{-/-}/Aass^{-/-}$) mouse strain. In brief, 1×10^6 hepatocytes were injected into the spleen of 2-month-old mice (male and female). Immediately after transplantation, selection pressure towards transplanted hepatocytes was applied by withdrawing the drug nitisinone (NTBC) from drinking water. After 2 weeks, mice were returned to NTBC treatment for 3 days before a second withdrawal (cycling). Subsequently, mice remained without nitisinone for 6 months to assure a good repopulation with transplanted hepatocytes. Before starting the high-protein diet challenge, mice were placed on NTBC to ensure no interference with the tyrosinemia in the TIRF strain. Aged-matched (8-month-old) corresponding controls were used for all transplant experiments.

AAV vector cloning and AAV virus production

Murine *Gcdh* cDNA was cloned by removing EmGFP in the 1162-pAAV-HLP-EmGFP-SpA plasmid (Addgene) using *XbaI-MluI* restriction enzymes. Murine *Aass* Sa sgRNAs oligonucleotides were annealed and ligated into 1313.1- pAAV-U6-SA-BbsI-MluI-gRNA-HLP-OLLAS-spA vector (Addgene #109314) with *BbsI* restriction enzyme. AAVs were produced as previously described (28) using the AAVcc47 capsid (29). *S. aureus* sgRNAs sequences used to target exons 6 and 7 of *mAass* are 5’ GTCCCTGTGAAGACAAACGTT 3’ (- strand) and 5’ CTTGTGAGTATGTGGAGCCCC 3’ (+ strand), respectively.

siRNA experiments and preparation

siRNA injection solution was prepared following Invivofectamine 3.0 Reagent Complexation protocol (Thermosfisher Scientific). In brief, siRNA duplex (sense sequence 5' GGAGUCUUGAUGAACAUAAtt 3' and antisense sequence 5' UUAUGUUCAUCAAGACUCCca 3', Ambion, Cat#4457308, ID#s78304) was first diluted in RNAse free water to a concentration of 250μM, aliquoted and stored at −80°C. siRNA duplex solution was diluted in 1:1 in complexation buffer and then mixed 1:1 with Invivofectamine 3.0 Reagent, vortexed, and incubated at 50°C for 30 minutes. The complex was diluted 1:6 with RNAse PBS1x pH7.4.

Aass siRNA (8mg/kg) solution was injected into the tail vein of 3-week-old $Gcdh^{-/-}$ mice that were put on a high protein diet 48 hours later. Mice were harvested postmortem for protein expression of AASS in the liver using AASS immunostaining as described in the immunostaining section method.

Neurobehavioral studies

Mouse motor activity studies were conducted by staff in the Mouse Behavioral and Neuroendocrine Core Facility at Duke University.

Spontaneous motor activity: Spontaneous motor activity was monitored in the open field (21 × 21 × 30 cm) over 30 min in an automated Omnitech Digiscan apparatus (AccuScan Instruments) (30). The Accuscan software scored motor activities as horizontal or vertical beam-breaks to determine the total distance traveled, vertical activity, velocity of movement, and time spent in the center zone of the arena.

Accelerating rotarod: Balance and coordination were evaluated on an accelerating (4–40 rpm over 5-min) rotarod (Med-Associates) as described (31). Motor performance was examined over 4 successive 5-min trials that were separated by 20–30 min each. A given trial was terminated when the mouse fell from the rod or when 300 sec had elapsed, and these times were recorded as the latency to fall.

Grip strength: The strength of the front and rear paws to grip a bar was analyzed with a mouse grip-strength meter (San Diego Instruments) and was expressed as units of g-force (32).

Blood Metabolite Analysis

Acylcarnitine (C5-DC) and amino acids (lysine and tryptophan) were measured from whole blood obtained from mice by retro-orbital eye bleeding four days after high-protein diet exposure.

Blood acylcarnitine (C5-DC)

Materials: Whatman 903 protein saver cards (Sigma-Aldrich), d_3-Acetylcarnitine (d_3-C2, Sigma-Aldrich) d_3-Propionylcarnitine (d_3-C3, Sigma-Aldrich), d_3-Butyrylcarnitine (d_3-C4, Sigma-Aldrich), d_3-Octanoylcarnitine (d_3-C8, Sigma-Aldrich) and d_3-Palmitoylcarnitine (d_3-C16, Sigma-Aldrich). General solvents and reagents were purchased from Sigma-

Aldrich or VWR. In-house deionized water (diH_2O) was used in the preparation of mobile phases or for dilutions.

Sample preparation: Whole blood (16 μL) was pipetted onto two 3/16" diameter circles of cotton-fiber filter paper and allowed to dry overnight in a microcentrifuge tube. Subsequently, 6 μL of an internal standard (IS) mixture [5 μmol/L d_3-C2, 1 μmol/L d_3-C3, 1 μmol/L d_3-C4, 1 μmol/L d_3-C8, 2 μmol/L d_3-C16 in methanol: diH_2O 50:50 (v/v)] was added to the tube with 400 μL of methanol (MeOH). The microcentrifuge tubes were placed on an orbital shaker for 30 min at ambient temperature. The entire volume of liquid was transferred to a 0.2 μm filter tube and centrifuged at 16,380 x g for 2 min. An aliquot (200 μL) of the filtered supernatant was transferred to a 96-well round-bottom plate and evaporated to dryness under nitrogen at 40°C. After drying, 70 μL of 3M MeOH-hydrochloric acid was added to each well, an adhesive cover was placed over each plate, and the samples incubated in an oven for 15 min at 50°C. Samples were dried under a stream of nitrogen at 40°C and reconstituted in a matrix of MeOH:diH_2O 85:15 (v:v) and analyzed by electrospray ionization-tandem mass spectrometry (ESI-MS/MS) (33, 34).

LC-MS/MS Analysis: Acylcarnitines in whole blood were analyzed as methyl esters using stable isotope dilution ESI-MS/MS. Derivatized samples were analyzed by flow injection analysis (FIA) and detected using a precursor ion scan of m/z 99. Samples were analyzed using a TQ Detector tandem-quadrupole mass spectrometer equipped with an Acquity Classic system (Waters Corporation). A FIA was performed over 2.5 min using MeOH:diH_2O 80:20 (v:v), which permitted elution of the sample between 0.2 and 1.0 min, with a wash-out period between 1.0 and 2.2 min, followed by a re-equilibration period from 2.2 to 2.5 min.

Data Processing: The raw data were processed using Neolynx (Waters Corp.). The ratio of ion intensities of acylcarnitine species and its specified deuterated IS was multiplied by the nominal concentration of the IS (5, 1, 1, 1, 2 μmol/L). Concentrations of standards are given in units of μmol/L. Glutarylcarnitine (C5-DC), with a m/z 304, was measured against octanoyl-L-carnitine-d_3 (d_3-C8) with m/z 305. Propionylcarnitine (C3), with m/z 232, and acetylcarnitine (C2), with m/z 218, were each compared to their own deuterated IS (d_3-C2 and d_3-C3).

Blood Amino Acids

Materials: Whatman 903 protein saver cards (Sigma-Aldrich), Kairos amino acid internal standard set (100+), amino acid calibrator set (100+), amino acid quality control set (100+), and the AccQ-Tag Ultra derivatization kit were purchased from Waters Corporation LC-MS grade acetonitrile, methanol, formic acid, acids and bases were purchased from Sigma-Aldrich or VWR. In-house deionized water (diH2O) was used in the preparation of mobile phases or for dilutions.

Analysis of amino acids by LC-MS/MS: Whole blood (12 μL) was pipetted onto a 1/4" diameter circle of cotton-fiber filter paper and allowed to dry overnight in a microcentrifuge tube. Plasma amino acids were analyzed using a modification of the Kairos Amino Acid

method. Equal volumes (50 μL) of plasma and an internal standard solution containing a mixture of [^{13}C, ^{15}N]-labeled amino acids were combined. Protein was precipitated using 50 μL 10% sulfosalicylic acid and removed by centrifugation. The supernatant was added to a borate buffer, mixed with the 6-aminoquinolyl-N-hydroxysuccinimidyl carbamate (AQC) derivatization reagent, incubated at 55 °C for 10 min, and diluted with dH_2O. Plasma amino acid-AQC derivatives were analyzed using a Waters Acquity I-Class UPLC coupled to a Waters Xevo TQ-S micro mass spectrometer. Amino acids were separated on a 1.6 μm 2 × 150 mm Cortecs UPLC column by gradient elution over 9.5 min, with 0.1% formic acid in aqueous acetonitrile as the mobile phase. Analytes were detected by selected reaction monitoring in positive ion mode. Peak area ratios of amino acids and their corresponding internal standard were converted to a concentration by means of a 6- or 7-point 1/x weighted calibration curve. Details of the acquisition parameters and calibrator concentrations are provided in tables S1 and S2.

Tissue organic acids

100mg of liver and brain tissues were obtained from mice at harvesting endpoint followed by homogenization in 500ml of distilled water.

Glutaric acid and 3-OH glutaric acid measurements: Quantitative measurement of glutaric acid (GA) and 3-OH-glutaric acid (3-OH-GA) in tissue homogenates was performed by gas chromatography–mass spectroscopy using stable-isotope dilution as previously described (35). Samples were sonicated for 20 cycles. Seventy mg of sulfosalicylic acid was added to the samples to remove endogenous protein. Samples were centrifuged at 13120 rpm for 20 min (desktop centrifuge). One-half mL of the resulting supernatant was removed and the deuterated internal standards (100 μL d4 glutaric and 12.5 μL d5 3H glutaric acid) were added. The mixture was extracted twice with 3 mL diethyl ether and 1.5 mL ethyl acetate. The combined organic phases were dried at 30°C under nitrogen and derivatized with 100 μL BTSFA/1% TMCS [N,O-Bis(trimethylsilyl)trifluoroacetamide with trimethylchlorosilane] for 20 min at 80°C. The injected volume of 1 μL was analyzed using an Agilent Technologies 6890N Gas Chromatograph equipped with a 5973N Mass Selective Detector. The mass spectrometer monitored ions at 265/261 (with check of ratio at 237/ 233) for GA and 262/259 (check ratio at 188/185) for 3-OH-GA in separate runs. Quantitation was performed against a separate standard curve for each compound (0 to 10 μg).

Immunohistochemistry

Paraffin-embedded slides were deparaffinated, rehydrated, and treated with antigen retrieval citrate buffer (p H6.0) (for RFP, AASS and FAH) or with Tris-EDTA buffer (pH 9) (Abcam) antigen retrieval (for GCDH) for 30 min at 98°C degrees. Endogenous peroxidase was quenched using 3% hydrogen peroxidase solution (Sigma-Aldrich) and biotin was blocked using the Avidin/Biotin kit following manufacturer's instructions (Vector Laboratories). After blocking with serum (PK-4001), samples were incubated with either rabbit anti-RFP (Rockland, cat# 600–401-379), rabbit anti-AASS (Sigma-Aldrich, cat# HPA020728), GCDH (Sigma Aldrich, cat# AV43559) or rabbit anti-human FAH antibodies (Sigma Aldrich, SAB2108553) primary antibodies diluted 1:100 in antibody diluent buffer (Abcam) and incubated overnight at 4°C. Slides were washed 2x with PBS1x for 15 min and

incubated with the anti-rabbit biotinylated secondary antibody at room temperature for 30 min. Immunostaining was developed with a DAB kit (Vector Laboratories). Counterstaining was performed using hematoxylin solution (Richard-Allan Scientific) and bluing solution (Richard-Allan Scientific). Cytoseal (Epredia) was used for mounting slides.

Western blot

Twenty grams of fresh-frozen liver and brain tissues were homogenized with 1.2 mL RIPA buffer (Sigma Aldrich) containing protease inhibitors (Roche, cat# 04693159001). Twenty μL (corresponding to 10 μg of protein) of homogenized samples were pre-mixed with loading buffer, heated, and loaded into wells of a polyacrylamide pre-made gel (NuPAGE 4–12% Bis Tris Gel Invitrogen) and transferred to a PDVF membrane (Millipore). After blocking (EveryBlot Blocking Buffer, Biorad) for 30 min, membranes were incubated at 4°C overnight with primary antibodies diluted in PBS-T. Rabbit Anti-AASS (Sigma-Aldrich, HPA020728), anti-GCDH (Sigma-Aldrich, HPA020728), and β-actin (Sigma Aldrich, A1978) were diluted 1:1,000. After washing, membranes were incubated with donkey anti-rabbit HRP secondary antibody (Jackson Immunoresearch, 711–035-152; diluted 1:5,000) for 1 hour at room temperature. The images were obtained by incubating the membranes with Super Signal West Fempto solution (Thermofisher).

Histopathology

Selected tissues (liver, lung, heart, kidney, spleen, and brain) were evaluated by a board-certified veterinary pathologist (J.I.E) in a blinded fashion without knowledge of the allocation group. Mouse brains were sectioned in the parasagittal plane. After identification of two lesions in initial screening, (meningeal hemorrhage & hippocampal vacuolation), the pathologist graded changes in the brains as normal, minimal, mild, moderate or severe (0–4) using a semi-quantitative scale considering not only the number but also the size/extension of the pathological findings. The whole hippocampus (parasagittal sections) was evaluated for scoring of vacuolation and the whole brain for meningeal hemorrhage. One grade was given for each mouse lesion.

Statistical analysis

Statistics are described in the text for individual experiments. Data are expressed as mean ± S.E.M. unless otherwise indicated. Statistical analysis and graphs were done using PRISM (Graph Pad) version 9 software. For comparison of two groups, the Student's *t*-tests were used when samples were normally distributed (analyzed with Shapiro-Wilk test); Mann-Whitney *U* test was used when non-parametric. Motor performance repeated-measures were analyzed with ANOVA (RMANOVA) followed by Bonferroni corrected pair-wise comparisons. p-values of <0.05 (*), <0.01 (**) or >0.001 (***) were considered significant. A log-rank (Mantel-Cox) test was used for the survival curve in fig. S10 ($p<0.05$). We did not find differences between male and female mice in regard to biochemical and clinical endpoints on high-protein diet, and therefore used both sexes in equal numbers.

Supplementary Material

Refer to Web version on PubMed Central for supplementary material.

Acknowledgments:

We thank the Genetically Engineered Rodent Models (GERM) Core at BCM for help with generation of the knockout mouse models, Chris Means from the mouse behavioral and Neuroendocrine Analysis Core Facility at Duke for help with behavioral experimentation and Katherine Misuraca for critical comments on the manuscript.

Funding:

The Alice and Y. T. Chen Center for Genetics and Genomics (to K.-D.B. and A.E.-G.), National Institute of Diabetes and Digestive and Kidney Disease (DK115461 to K.D.B.; DK124477 to W.R.L.; T32DK060445 to C.G.J), National Heart Lung and Blood Institute (HL132840 to W.R.L.; R01HL089221 to A.A.). and National Institute of General Medical Sciences (T32GM088129 to C.G.J.)

Data and materials availability:

All data is available in the manuscript or the supplementary materials.

References:

1. Goodman SI, Markey SP, Moe PG, Miles BS, Teng CC, Glutaric aciduria; a “new” disorder of amino acid metabolism. Biochem Med 12, 12–21 (1975); published online EpubJan (10.1016/0006-2944(75)90091-5). [PubMed: 1137568]
2. Larson A, Goodman S, in GeneReviews((R)), Adam MP, Everman DB, Mirzaa GM, Pagon RA, Wallace SE, Bean LJH, Gripp KW, Amemiya A, Eds. (Seattle (WA), 1993).
3. Strauss KA, Morton DH, Type I glutaric aciduria, part 2: a model of acute striatal necrosis. American journal of medical genetics. Part C, Seminars in medical genetics 121C, 53–70 (2003); published online EpubAug 15 (10.1002/ajmg.c.20008). [PubMed: 12888986]
4. Boy N, Mengler K, Heringer-Seifert J, Hoffmann GF, Garbade SF, Kolker S, Impact of newborn screening and quality of therapy on the neurological outcome in glutaric aciduria type 1: a meta-analysis. Genet Med 23, 13–21 (2021); published online EpubJan (10.1038/s41436-020-00971-4). [PubMed: 32981931]
5. Sauer SW, Okun JG, Fricker G, Mahringer A, Muller I, Crnic LR, Muhlhausen C, Hoffmann GF, Horster F, Goodman SI, Harding CO, Koeller DM, Kolker S, Intracerebral accumulation of glutaric and 3-hydroxyglutaric acids secondary to limited flux across the blood-brain barrier constitute a biochemical risk factor for neurodegeneration in glutaryl-CoA dehydrogenase deficiency. J Neurochem 97, 899–910 (2006); published online EpubMay (10.1111/j.1471-4159.2006.03813.x). [PubMed: 16573641]
6. Strauss KA, Williams KB, Carson VJ, Poskitt L, Bowser LE, Young M, Robinson DL, Hendrickson C, Beiler K, Taylor CM, Haas-Givler B, Hailey J, Chopko S, Puffenberger EG, Brigatti KW, Miller F, Morton DH, Glutaric acidemia type 1: Treatment and outcome of 168 patients over three decades. Molecular genetics and metabolism 131, 325–340 (2020); published online EpubNov (10.1016/j.ymgme.2020.09.007). [PubMed: 33069577]
7. Bouchereau J, Schiff M, Inherited Disorders of Lysine Metabolism: A Review. J Nutr 150, 2556S–2560S (2020); published online EpubOct 1 (10.1093/jn/nxaa112). [PubMed: 33000154]
8. Manoli I, Venditti CP, Disorders of branched chain amino acid metabolism. Transl Sci Rare Dis 1, 91–110 (2016); published online EpubNov 7 (10.3233/TRD-160009). [PubMed: 29152456]
9. Mitchell G, Larochelle J, Lambert M, Michaud J, Grenier A, Ogier H, Gauthier M, Lacroix J, Vanasse M, Larbrisseau A, et al. , Neurologic crises in hereditary tyrosinemia. N Engl J Med 322, 432–437 (1990); published online EpubFeb 15 (10.1056/NEJM199002153220704). [PubMed: 2153931]
10. Koeller DM, Woontner M, Crnic LS, Kleinschmidt-DeMasters B, Stephens J, Hunt EL, Goodman SI, Biochemical, pathologic and behavioral analysis of a mouse model of glutaric acidemia type I. Hum Mol Genet 11, 347–357 (2002); published online EpubFeb 15 (10.1093/hmg/11.4.347). [PubMed: 11854167]

11. Zinnanti WJ, Lazovic J, Wolpert EB, Antonetti DA, Smith MB, Connor JR, Woontner M, Goodman SI, Cheng KC, A diet-induced mouse model for glutaric aciduria type I. Brain 129, 899–910 (2006); published online EpubApr (10.1093/brain/awl009). [PubMed: 16446282]
12. Zinnanti WJ, Lazovic J, Housman C, Antonetti DA, Koeller DM, Connor JR, Steinman L, Mechanism of metabolic stroke and spontaneous cerebral hemorrhage in glutaric aciduria type I. Acta Neuropathol Commun 2, 13 (2014); published online EpubJan 27 (10.1186/2051-5960-2-13). [PubMed: 24468193]
13. Sauer SW, Opp S, Komatsuzaki S, Blank AE, Mittelbronn M, Burgard P, Koeller DM, Okun JG, Kolker S, Multifactorial modulation of susceptibility to l-lysine in an animal model of glutaric aciduria type I. Biochim Biophys Acta 1852, 768–777 (2015); published online EpubMay (10.1016/j.bbadis.2014.12.022). [PubMed: 25558815]
14. Bissig-Choisat B, Alves-Bezerra M, Zorman B, Ochsner SA, Barzi M, Legras X, Yang D, Borowiak M, Dean AM, York RB, Galvan NTN, Goss J, Lagor WR, Moore DD, Cohen DE, McKenna NJ, Sumazin P, Bissig KD, A human liver chimeric mouse model for non-alcoholic fatty liver disease. JHEP Rep 3, 100281 (2021); published online EpubJun (10.1016/j.jhepr.2021.100281).
15. Barzi M, Pankowicz FP, Zorman B, Liu X, Legras X, Yang D, Borowiak M, Bissig-Choisat B, Sumazin P, Li F, Bissig KD, A novel humanized mouse lacking murine P450 oxidoreductase for studying human drug metabolism. Nature communications 8, 39 (2017); published online EpubJun 28 (10.1038/s41467-017-00049-x).
16. Leandro J, Dodatko T, DeVita RJ, Chen H, Stauffer B, Yu C, Houten SM, Deletion of 2-aminoadipic semialdehyde synthase limits metabolite accumulation in cell and mouse models for glutaric aciduria type 1. Journal of inherited metabolic disease 43, 1154–1164 (2020); published online EpubNov (10.1002/jimd.12276). [PubMed: 32567100]
17. McMillan TA, Gibson KM, Sweetman L, Meyers GS, Green R, Conservation of central nervous system glutaryl-coenzyme A dehydrogenase in fruit-eating bats with glutaric aciduria and deficient hepatic glutaryl-coenzyme A dehydrogenase. J Biol Chem 263, 17258–17261 (1988); published online EpubNov 25 ([PubMed: 3182847]
18. Pena IA, Marques LA, Laranjeira AB, Yunes JA, Eberlin MN, MacKenzie A, Arruda P, Mouse lysine catabolism to aminoadipate occurs primarily through the saccharopine pathway; implications for pyridoxine dependent epilepsy (PDE). Biochim Biophys Acta Mol Basis Dis 1863, 121–128 (2017); published online EpubJan (10.1016/j.bbadis.2016.09.006). [PubMed: 27615426]
19. Consortium GT, Human genomics. The Genotype-Tissue Expression (GTEx) pilot analysis: multitissue gene regulation in humans. Science 348, 648–660 (2015); published online EpubMay 8 (10.1126/science.1262110). [PubMed: 25954001]
20. Jafari P, Braissant O, Bonafe L, Ballhausen D, The unsolved puzzle of neuropathogenesis in glutaric aciduria type I. Molecular genetics and metabolism 104, 425–437 (2011); published online EpubDec (10.1016/j.ymgme.2011.08.027). [PubMed: 21944461]
21. Pankowicz FP, Jarrett KE, Lagor WR, Bissig KD, CRISPR/Cas9: at the cutting edge of hepatology. Gut 66, 1329–1340 (2017); published online EpubJul (10.1136/gutjnl-2016-313565). [PubMed: 28487442]
22. Pankowicz FP, Barzi M, Legras X, Hubert L, Mi T, Tomolonis JA, Ravishankar M, Sun Q, Yang D, Borowiak M, Sumazin P, Elsea SH, Bissig-Choisat B, Bissig KD, Reprogramming metabolic pathways in vivo with CRISPR/Cas9 genome editing to treat hereditary tyrosinaemia. Nature communications 7, 12642 (2016)10.1038/ncomms12642).
23. Nguyen GN, Everett JK, Kafle S, Roche AM, Raymond HE, Leiby J, Wood C, Assenmacher CA, Merricks EP, Long CT, Kazazian HH, Nichols TC, Bushman FD, Sabatino DE, A long-term study of AAV gene therapy in dogs with hemophilia A identifies clonal expansions of transduced liver cells. Nat Biotechnol 39, 47–55 (2021); published online EpubJan (10.1038/s41587-020-0741-7). [PubMed: 33199875]
24. Donsante A, Miller DG, Li Y, Vogler C, Brunt EM, Russell DW, Sands MS, AAV vector integration sites in mouse hepatocellular carcinoma. Science 317, 477 (2007); published online EpubJul 27 (10.1126/science.1142658). [PubMed: 17656716]

25. Muhlhausen C, Ergun S, Strauss KA, Koeller DM, Crnic L, Woontner M, Goodman SI, Ullrich K, Braulke T, Vascular dysfunction as an additional pathomechanism in glutaric aciduria type I. Journal of inherited metabolic disease 27, 829–834 (2004)10.1023/B:BOLI.0000045766.98718.d6). [PubMed: 15505389]
26. Maeso-Diaz R, Dalton GD, Oh S, Du K, Tang L, Chen T, Dutta RK, Hartman JH, Meyer JN, Diehl AM, Aging reduces liver resiliency by dysregulating Hedgehog signaling. Aging Cell 21, e13530 (2022); published online EpubFeb (10.1111/acel.13530).
27. Bissig-Choisat B, Wang L, Legras X, Saha PK, Chen L, Bell P, Pankowicz FP, Hill MC, Barzi M, Leyton CK, Leung HC, Kruse RL, Himes RW, Goss JA, Wilson JM, Chan L, Lagor WR, Bissig KD, Development and rescue of human familial hypercholesterolaemia in a xenograft mouse model. Nature communications 6, 7339 (2015)10.1038/ncomms8339).
28. Nelson CE, Wu Y, Gemberling MP, Oliver ML, Waller MA, Bohning JD, Robinson-Hamm JN, Bulaklak K, Castellanos Rivera RM, Collier JH, Asokan A, Gersbach CA, Long-term evaluation of AAV-CRISPR genome editing for Duchenne muscular dystrophy. Nat Med 25, 427–432 (2019); published online EpubMar (10.1038/s41591-019-0344-3). [PubMed: 30778238]
29. Gonzalez TJ, Simon KE, Blondel LO, Fanous MM, Roger AL, Maysonet MS, Devlin GW, Smith TJ, Oh DK, Havlik LP, Castellanos Rivera RM, Piedrahita JA, ElMallah MK, Gersbach CA, Asokan A, Cross-species evolution of a highly potent AAV variant for therapeutic gene transfer and genome editing. Nature communications 13, 5947 (2022); published online EpubOct 10 (10.1038/s41467-022-33745-4).
30. Fukui M, Rodriguiz RM, Zhou J, Jiang SX, Phillips LE, Caron MG, Wetsel WC, Vmat2 heterozygous mutant mice display a depressive-like phenotype. J Neurosci 27, 10520–10529 (2007); published online EpubSep 26 (10.1523/JNEUROSCI.4388-06.2007). [PubMed: 17898223]
31. Taylor GA, Rodriguiz RM, Greene RI, Daniell X, Henry SC, Crooks KR, Kotloski R, Tessarollo L, Phillips LE, Wetsel WC, Behavioral characterization of P311 knockout mice. Genes Brain Behav 7, 786–795 (2008); published online EpubOct (10.1111/j.1601-183X.2008.00420.x). [PubMed: 18616608]
32. Wang X, McCoy PA, Rodriguiz RM, Pan Y, Je HS, Roberts AC, Kim CJ, Berrios J, Colvin JS, Bousquet-Moore D, Lorenzo I, Wu G, Weinberg RJ, Ehlers MD, Philpot BD, Beaudet AL, Wetsel WC, Jiang YH, Synaptic dysfunction and abnormal behaviors in mice lacking major isoforms of Shank3. Hum Mol Genet 20, 3093–3108 (2011); published online EpubAug 1 (10.1093/hmg/ddr212). [PubMed: 21558424]
33. Millington DS, Stevens RD, Acylcarnitines: analysis in plasma and whole blood using tandem mass spectrometry. Methods in molecular biology (Clifton, N.J 708, 55–72 (2011)10.1007/978-1-61737-985-7_3).
34. Lepage N, Aucoin S, Measurement of plasma/serum acylcarnitines using tandem mass spectrometry. Methods in molecular biology (Clifton, N.J 603, 9–25 (2010)10.1007/978-1-60761-459-3_2).
35. Zinnanti WJ, Lazovic J, Housman C, LaNoue K, O'Callaghan JP, Simpson I, Woontner M, Goodman SI, Connor JR, Jacobs RE, Cheng KC, Mechanism of age-dependent susceptibility and novel treatment strategy in glutaric acidemia type I. The Journal of clinical investigation 117, 3258–3270 (2007); published online EpubNov (10.1172/JCI31617). [PubMed: 17932566]

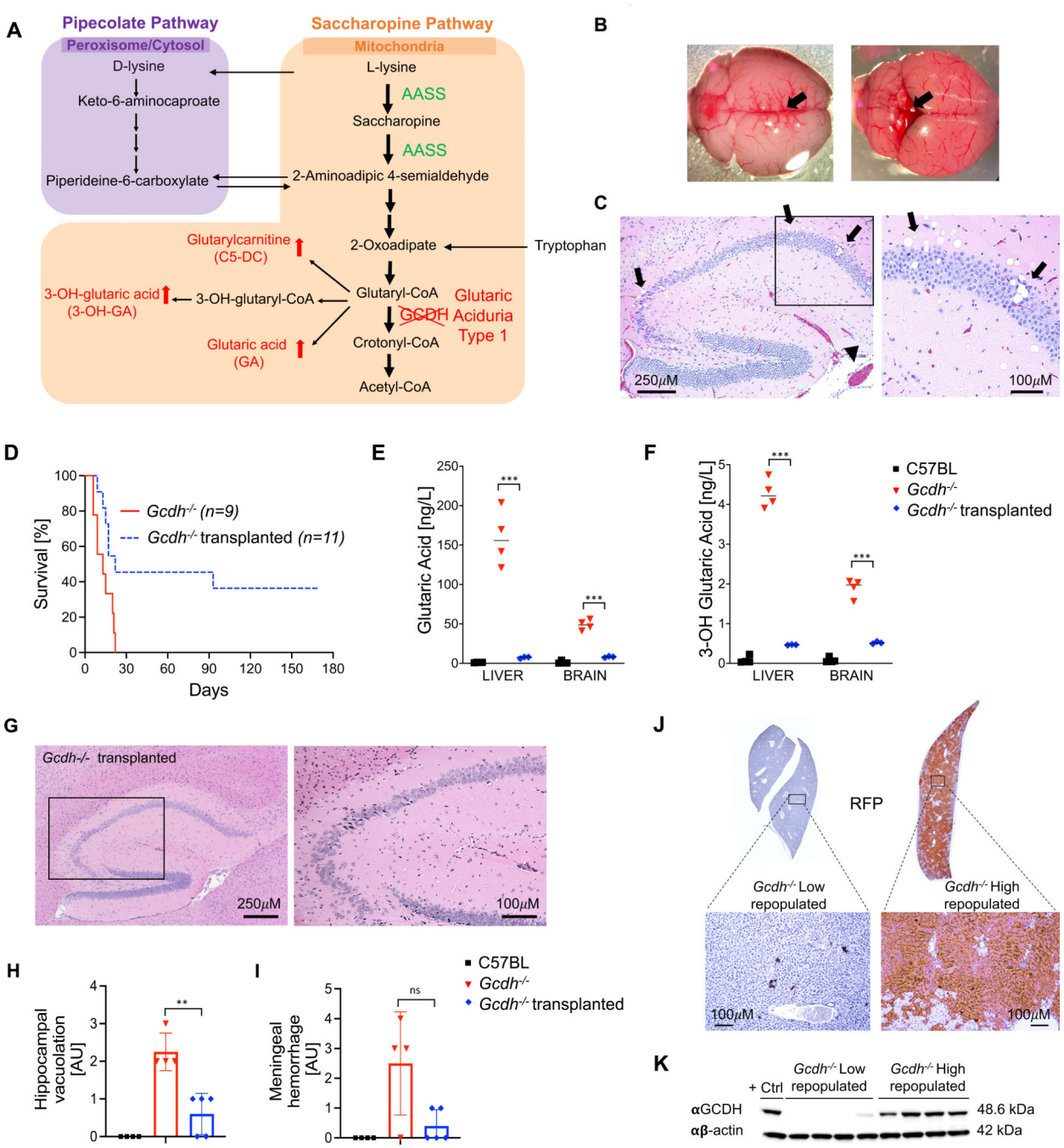

Figure 1. *Gcdh*$^{-/-}$ knockout mice: phenotype and rescue by hepatocyte transplantation.

(A) Known lysine catabolism pathway in peroxisomes, cytosol, and mitochondria. (**B**) Brain hemorrhage (arrow) of *Gcdh*$^{-/-}$ mice after 4 days on high-protein diet exposure. (**C**) Representative H&E staining of the hippocampus with vacuolation (arrow). Boxed area shown with higher magnification on the right. (**D**) Kaplan-Meier survival curves of *Gcdh*$^{-/-}$ knockout mice transplanted with wild-type hepatocytes (*Gcdh*$^{+/+}$) on high-protein diet. Glutaric acid (**E**) and 3-OH-glutaric acid (**F**) concentrations in liver and brain of groups after 10 (non-transplanted) or 160 (transplanted) days on high-protein diet. (**G**) H&E

staining of hippocampal brain sections. Boxed area shown with higher magnification on the right. Quantification of hippocampal vacuolation (**H**) and meningeal hemorrhage (**I**) (Arbitrary Units [AU]: 0 = absence; 1 = low; 2 = intermediate; 3 = high; 4 = very high). (**J**) RFP immunohistochemistry detecting healthy hepatocytes (*Gcdh*+/+, transgenic *mTmG*) and (**K**) Western blot (GCDH and beta actin) of liver lysates from low and high repopulated transplanted animals (n=4 per group). Data is presented as means ± SD. Significance was validated with Student's t test (D, E) or Mann-Whitney *U* test (H, I); *p≤0.05, **p≤0.01 and *** p≤0.005. All mice were transplanted at the age of 2 months and experiments were performed at age of 8 months. Non-transplanted controls were age-matched. GCDH: Glutaryl-Co-A Dehydrogenase; AASS: Alpha Aminoadipate-Semialdehyde Synthase; RFP: Red Fluorescent Protein; *mTmG*: membrane Tomato membrane GFP.

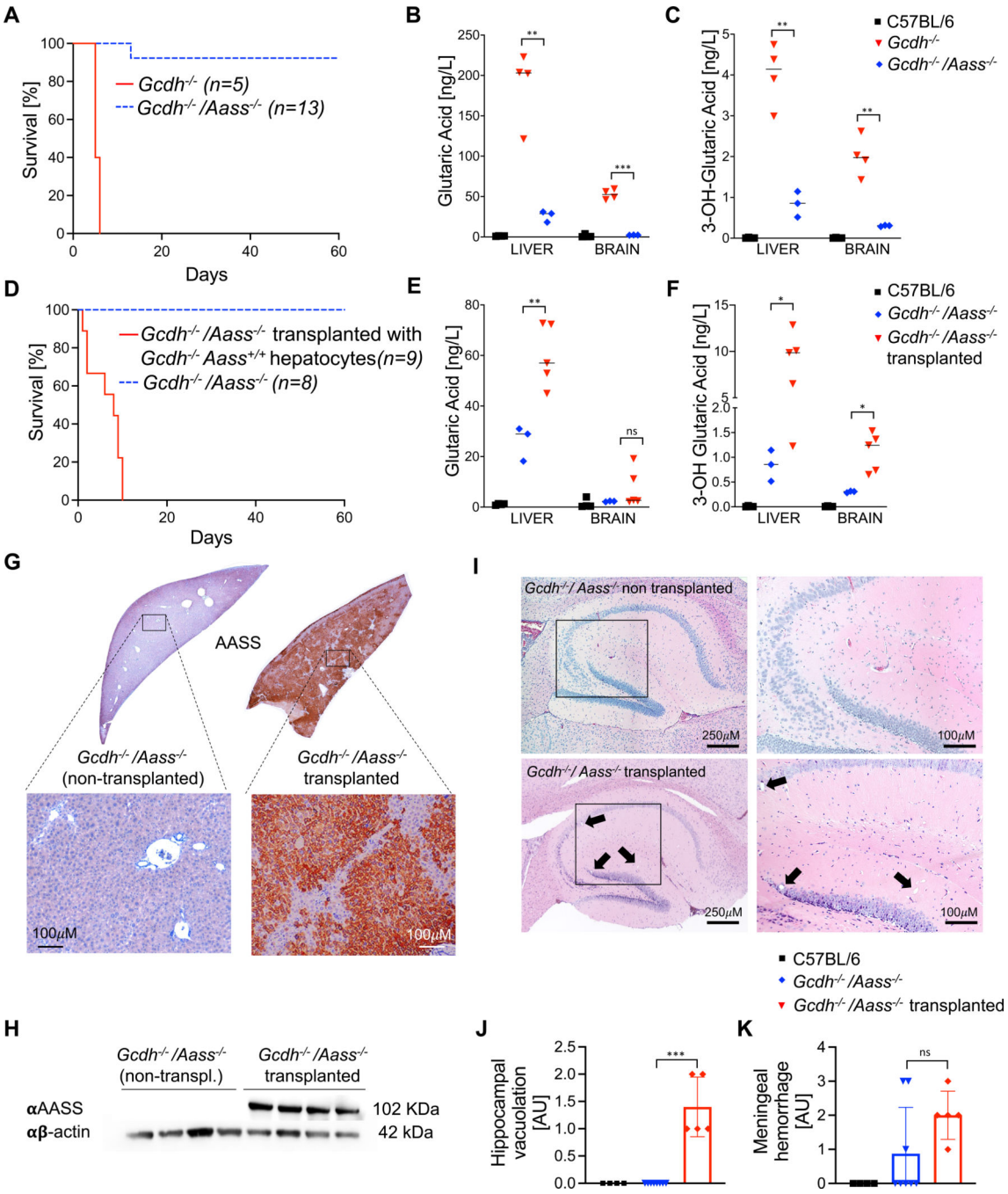

Figure 2. Phenotype and transplantation experiments of double knockout (*Gcdh*$^{-/-}$/*Aass*$^{-/-}$) mice.

(**A**) Kaplan-Meier survival curves of single (*Gcdh*$^{-/-}$) and double (*Gcdh*$^{-/-}$Aass$^{-/-}$) knockout mice on high-protein diet. (**B**-**C**) Glutaric acid (**B**) and 3-OH-glutaric acid (**C**) concentrations in liver and brain tissue of single (*Gcdh*$^{-/-}$) and double (*Gcdh*$^{-/-}$/*Aass*$^{-/-}$) knockout mice after 5 and 60 days on high-protein diet, respectively. (**D**) Kaplan-Meier survival curves of double (*Gcdh*$^{-/-}$/*Aass*$^{-/-}$) knockout mice transplanted with *Gcdh*$^{-/-}$ hepatocytes. Glutaric acid (**E**) and 3-OH-glutaric acid (**F**) concentrations in liver and brain of double knockout (*Gcdh*$^{-/-}$/*Aass*$^{-/-}$) groups after 5 days (transplanted) and 60 days (non-

transplanted), on high-protein diet. Representative AASS immunostaining (**G**) and Western blot (**H**) of livers from transplanted double (*Gcdh*$^{-/-}$/*Aass*$^{-/-}$) knockout mice. (**I**) H&E staining of hippocampal brain sections with vacuolation (arrows). Boxed area shown with higher magnification on the right. **(J-K)** Quantification of hippocampal vacuolation (**J**) and brain meningeal hemorrhage (**K**). Arbitrary Units (AU): 0 = absence; 1 = low; 2 = intermediate; 3 = high; 4 = very high. Data is presented as means ± SD. Significance was validated with t test (B, D) or with Mann-Whitney *U* test (H, J); *p≤0.05, **p≤0.01 and *** p≤0.005. All mice were transplanted at the age of 2 months and experiments were performed at age of 8 months. Non-transplanted controls were age-matched.

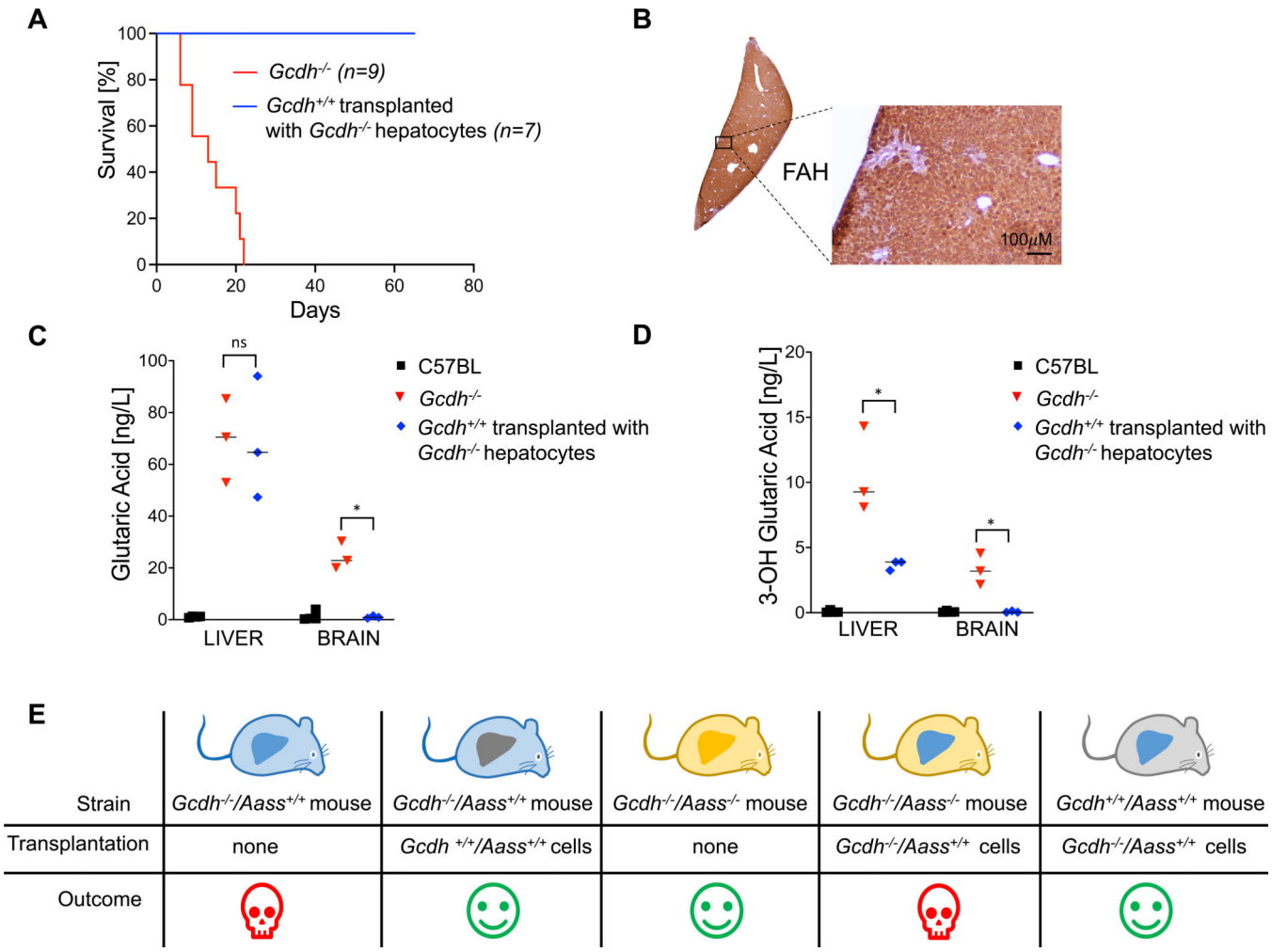

Figure 3. Phenotype of liver-specific GA-1 model.

Gcdh$^{-/-}$ hepatocytes were transplanted into TIRF (*transgene free Il2rg*$^{-/-}$*/Rag2*$^{-/-}$*/Fah*$^{-/-}$) mice, which have a normal lysine catabolism (*Gcdh*$^{+/+}$ */Aass*$^{+/+}$). (**A**) Kaplan Meier survival curve of TIRF mice transplanted with *Gcdh*$^{-/-}$ hepatocytes (**B**) Representative FAH immunohistochemistry of TIRF liver (FAH negative) transplanted with *Gcdh*$^{-/-}$ hepatocytes (FAH positive). Glutaric acid (**C**) and 3-OH-glutaric acid (**D**) concentrations in liver and brain of transplanted and non-transplanted mice on high protein diet. (**E**) Summary of hepatocyte transplantation models and their outcomes. Color codes for whole body and/or liver (transplanted hepatocytes) of mice in the diagram correspond to: Blue: *Gcdh*$^{-/-}$*/Aass*$^{+/+}$ (single knockout); Yellow: *Gcdh*$^{-/-}$*/Aass*$^{-/-}$ (double knockout); Grey: *Gcdh*$^{+/+}$*/Aass*$^{+/+}$(wild-type). Significance was validated with Mann-Whitney *U* test (*p≤0.05 and **p≤0.01). All mice were transplanted at the age of 2 months and experiments were performed at age of 8 months (see methods). Non-transplanted controls are age matched. Il2rg: Il-2 receptor gamma; Rag2: recombination activating gene 2; fah: fumarylacetoacetate hydrolase.

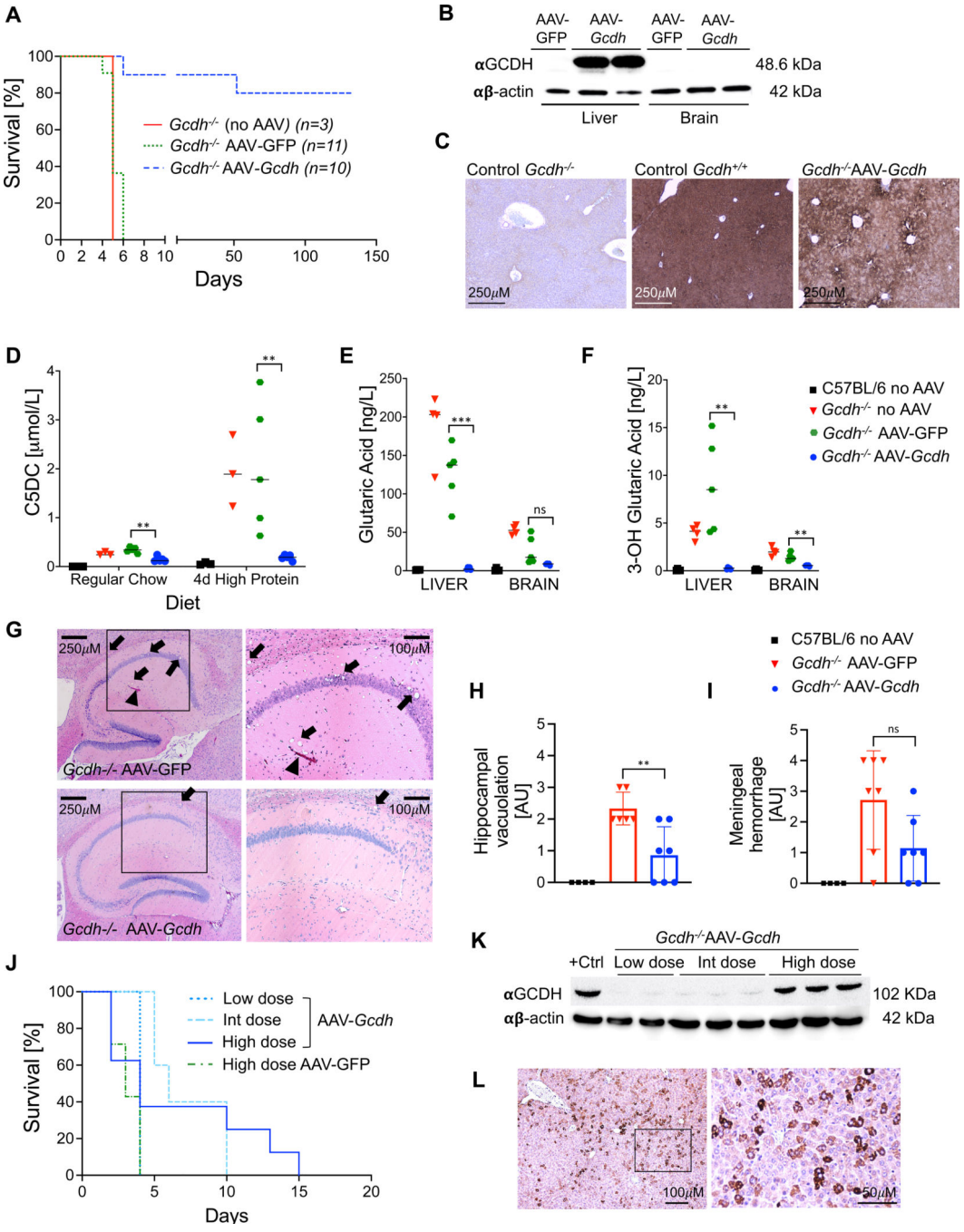

Figure 4. Liver-directed AAV gene therapy in *Gcdh*$^{-/-}$ mice.

(A-I) Five-week-old *Gcdh*$^{-/-}$ mice were intravenously injected with AAV-*Gcdh or* AAV-*GFP* at a dose of 1.5×10^{12} vg/mouse. (**A**) Kaplan Meier survival curves of *Gcdh*$^{-/-}$ mice on high-protein diet. (**B**) GCDH Western blot analysis of liver and brain lysates from AAV -treated mice after harvesting or expiration (controls). (**C**) Representative GCDH immunostaining of liver in treatment group. (**D**) C5-DC metabolite levels in whole blood of all experimental groups before and 4 days after high protein diet. Glutaric acid (**E**) and 3-OH-glutaric acid (**F**) concentrations in liver and brain tissue of *Gcdh*$^{-/-}$

mice at 140 days (AAV-*Gcdh*) or upon expiration (AAV-*GFP* and untreated). (**G**) H&E staining of hippocampal brain sections showing vacuolation (arrows) and meningeal hemorrhage (arrowheads). Boxed area shown with higher magnification on the right. **(H to I)** Quantification of hippocampal vacuolation (**H**) and brain meningeal hemorrhage (**I**). Arbitrary Units (AU): 0 = absence; 1 = low; 2 = intermediate; 3 = high; 4 = very high. (**J**-**K**) Neonatal $Gcdh^{-/-}$ pups treated with low (3×10^{11} vg/mouse), intermediate (7.5×10^{11} vg/mouse) and high (1.5×10^{12} vg/mouse) dose of AAV. (**J**) Kaplan Meier survival curves of treated $Gcdh^{-/-}$ mice on high protein after weaning. Western blot (**K**) and GCDH immunostaining (**L**) of treated (high dose) $Gcdh^{-/-}$ mice after expiration. Data is presented as means ± SD. Significance was validated with t-test (D,E,F) or Mann-Whitney *U* test (G,H); *p≤0.05, **p≤0.01 and ***p≤0.005. All mice were transplanted at the age of 2 months and experiments were performed at age of 8 months (see methods for details). Non-transplanted controls were age matched. AAV: Adeno-Associated Virus; C5-DC: glutarylcarnitine; GCDH: Glutaryl-Co-A Dehydrogenase.

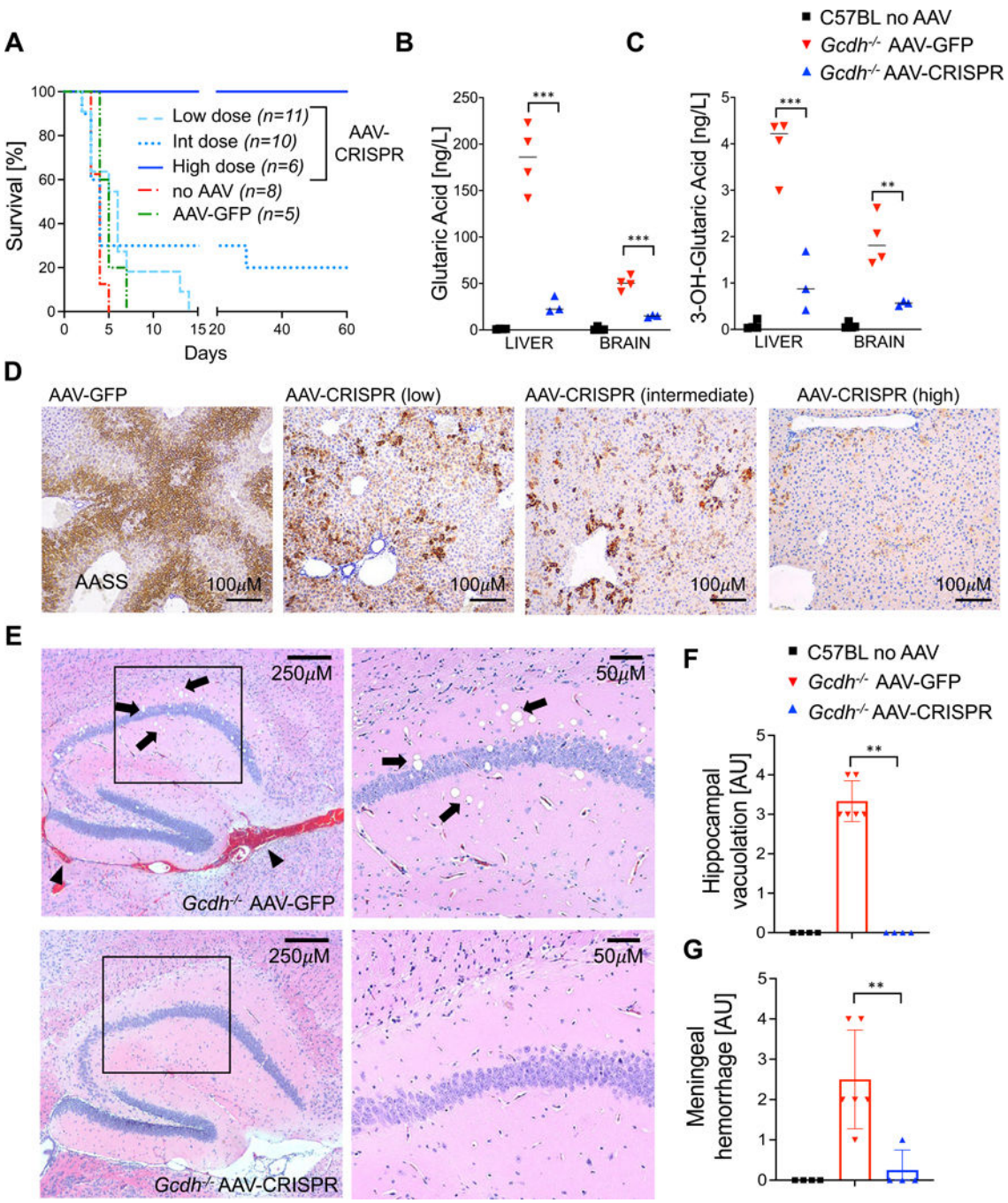

Figure 5. Liver-specific deletion of *Aass* in *Gcdh*$^{-/-}$ mice using AAV-CRISPR.

Neonatal *Gcdh*$^{-/-}$ mice were injected with a low (2.4×10^{11} vg/mouse), intermediate (6×10^{11} vg/mouse), or high (1×10^{12} vg/mouse) dose of AAV expressing Cas9 under a liver specific promoter and sgRNA targeting the *Aass* gene. (**A**) Kaplan Meier survival curves of experimental groups on high protein diet. Glutaric acid (**B**) and 3-OH-glutaric acid (**C**) concentrations in liver and brain of wild-type C57BL/6 mice and treated (AAV-CRISPR, *high dose*) *Gcdh*$^{-/-}$ mice after 60 days on high protein diet and upon expiration (day 4, AAV-*GFP*). (**D**) AASS immunostaining of livers of experimental groups (**E**)

Representative hippocampal sections of mice injected with *AAV*-CRISPR or *AAV-GFP* showing vacuolation (arrows) and hemorrhage (arrowheads). Quantification of hippocampal vacuolation (**F**) and meningeal hemorrhage (**G**). Data is presented as means ± SD. Significance was validated with t test (B) and with Mann-Whitney U test (D) (**p≤0.01, and ***p≤0.005 AAV: Adeno-Associated Virus; Gcdh: Glutaryl-Co-A Dehydrogenase. AASS: Alpha Aminoadipate-Semialdehyde Synthase.